



Chinese Pharmaceutical Association
Institute of Materia Medica, Chinese Academy of Medical Sciences

Acta Pharmaceutica Sinica B

www.elsevier.com/locate/apsb
www.sciencedirect.com



ORIGINAL ARTICLE

Discovery of a potent and highly selective inhibitor of SIRT6 against pancreatic cancer metastasis *in vivo*



Xinyuan Xu^{a,b,†}, Qian Zhang^{a,b,†}, Xufeng Wang^{c,†}, Jing Jin^{d,†},
Chengwei Wu^{a,b,†}, Li Feng^{a,b,e,†}, Xiuyan Yang^a, Mingzhu Zhao^{a,e},
Yingyi Chen^a, Shaoyong Lu^a, Zhen Zheng^a, Xiaobing Lan^f,
Yi Wang^{d,*}, Yan Zheng^{g,*}, Xuefeng Lu^{e,*}, Qiufen Zhang^{a,*},
Jian Zhang^{a,b,*}

^aState Key Laboratory of Medical Genomics, National Research Center for Translational Medicine at Shanghai, Ruijin Hospital, Shanghai Jiao Tong University School of Medicine, Shanghai 200025, China

^bMedicinal Chemistry and Bioinformatics Center, Shanghai Jiao Tong University School of Medicine, Shanghai 200025, China

^cDepartment of General Surgery, Huashan Hospital, Cancer Metastasis Institute, Fudan University, Shanghai 200040, China

^dInstitute of Immunology and the CAS Key Laboratory of Innate Immunity and Chronic Disease, School of Basic Medicine and Medical Center, University of Science and Technology of China, Hefei 230026, China

^eDepartment of Assisted Reproduction, Shanghai Ninth People's Hospital, Shanghai Jiao Tong University School of Medicine, Shanghai 200011, China

^fCollege of Pharmacy, Ningxia Medical University, Yinchuan 750004, China

^gDepartment of Pancreatic Surgery, Shanghai General Hospital, Shanghai Key Laboratory of Pancreatic Disease, Institute of Pancreatic Disease, Shanghai Jiao Tong University School of Medicine, Shanghai 200080, China

Received 17 July 2023; received in revised form 5 September 2023; accepted 18 October 2023

KEY WORDS

SIRT6;
Inhibitor;

Abstract Pancreatic cancer, one of the most aggressive malignancies, has no effective treatment due to the lack of targets and drugs related to tumour metastasis. SIRT6 can promote the migration of pancreatic cancer and could be a potential target for antimetastasis of pancreatic cancer. However, highly selective

*Corresponding authors.

E-mail addresses: wy83@ustc.edu.cn (Yi Wang), ygziling@126.com (Yan Zheng), xuefenglu163@163.com (Xuefeng Lu), autumn.sky@163.com (Qiufen Zhang), Jian.zhang@sjtu.edu.cn (Jian Zhang).

[†]These authors made equal contributions to this work.

Peer review under the responsibility of Chinese Pharmaceutical Association and Institute of Materia Medica, Chinese Academy of Medical Sciences.

<https://doi.org/10.1016/j.apsb.2023.11.014>

2211-3835 © 2024 The Authors. Published by Elsevier B.V. on behalf of Chinese Pharmaceutical Association and Institute of Materia Medica, Chinese Academy of Medical Sciences. This is an open access article under the CC BY-NC-ND license (<http://creativecommons.org/licenses/by-nc-nd/4.0/>).

Allosteric;
Selectivity;
Cocrystal;
Pancreatic cancer
metastasis

and potency SIRT6 inhibitor that can be used *in vivo* is yet to be discovered. Here, we developed a novel SIRT6 allosteric inhibitor, compound **11e**, with maximal inhibitory potency and an IC₅₀ value of $0.98 \pm 0.13 \mu\text{mol/L}$. Moreover, compound **11e** exhibited significant selectivity against other histone deacetylases (HDAC1–11 and SIRT1–3) at concentrations up to 100 $\mu\text{mol/L}$. The allosteric site and the molecular mechanism of inhibition were extensively elucidated by cocrystal complex structure and dynamic structural analyses. Importantly, we confirmed the antimetastatic function of such inhibitors in four pancreatic cancer cell lines as well as in two mouse models of pancreatic cancer liver metastasis. To our knowledge, this is the first study to reveal the *in vivo* effects of SIRT6 inhibitors on liver metastatic pancreatic cancer. It not only provides a promising lead compound for subsequent inhibitor development targeting SIRT6 but also provides a potential approach to address the challenge of metastasis in pancreatic cancer.

© 2024 The Authors. Published by Elsevier B.V. on behalf of Chinese Pharmaceutical Association and Institute of Materia Medica, Chinese Academy of Medical Sciences. This is an open access article under the CC BY-NC-ND license (<http://creativecommons.org/licenses/by-nc-nd/4.0/>).

1. Introduction

The sirtuin family is classified as class III histone deacetylases (HDACs) that employ NAD⁺ as a cofactor¹. However, sirtuins (SIRT) are capable of catalysing different reactions and possess a wide range of histones and nonhistone substrates². SIRT6, a nuclear member of the SIRT family, tightly regulates DNA repair and genome maintenance by deacetylating histone H3 N^ε-acetyl-lysines 9 (H3K9Ac)³, 56 (H3K56Ac)⁴, and 18 (H3K18Ac)⁵ at target gene promoters and by physically interacting with nonhistone transcription factors, such as NF- κ B⁶ and MYC⁷. The function is highly related to the roles of SIRT6 in ageing, metabolism, inflammation, and tumorigenesis^{8–11}. Given the multiple roles of SIRT6 in regulating the various cellular processes described above, the relationship of SIRT6 with cancer has been widely investigated over the past decades. Various studies have shown that SIRT6 plays a dual role as an oncogene or a tumour suppressor in a cell-specific and context-specific manner¹². SIRT6 expression was detected at lower levels in tumour tissues of hepatocellular carcinoma, colon cancer, lung cancer, ovarian cancer and glioma, and SIRT6 downregulation was associated with increased tumour progression^{7,13–15}. In contrast, SIRT6 expression was abnormally upregulated and accompanied by poor prognosis in several other types of cancer, including pancreatic cancer, prostate cancer, breast cancer, leukaemia, and melanoma^{16–22}, which reveals the potential oncogenic role of SIRT6. Overall, the diverse roles of SIRT6 in different cancer contexts predict the complexity of its clinical localization.

Pancreatic cancer is one of the most aggressive malignancies. Metastasis is a hallmark of pancreatic cancer and the major cause of death in cancer patients^{23,24}. More than half of pancreatic cancer patients are diagnosed with distant metastasis, with the liver being the most common site of pancreatic cancer metastasis^{25,26}. Surgical resection and chemotherapy remain the only effective approaches for pancreatic cancer patients to obtain a cure and long-term survival, although the 5-year survival rate is still less than 10% due to significant metastases and drug resistance^{27,28}. Therefore, druggable targets to prevent pancreatic cancer metastasis are urgently needed. Recently, SIRT6 silencing was found to eliminate the migration ability of BxPC-3 pancreatic cancer cells²². Through the deacetylation of histone H3K9Ac, SIRT6 leads to increased expression of the proinflammatory cytokines IL-8 and TNF- α as well as an enhanced intracellular Ca²⁺ response, which have been shown to play key roles in pancreatic

cancer metastasis^{29–32}. Thus, SIRT6 could serve as an unexplored druggable target, and SIRT6 inhibitors may provide a promising approach to prevent pancreatic cancer metastasis.

Due to the deficiencies in the activity and pharmacokinetics of inhibitors, the *in vivo* pharmacological activities of SIRT6 inhibitors in pancreatic cancer-induced metastasis remain unknown (Supporting Information Fig. S1). For example, endogenous ligands (*e.g.*, nicotinamide)³³ or natural products (*e.g.*, trichostatin A)³⁴ invariably showed nonselective activities against a range of HDAC family members, and other synthetic compounds from high-throughput screening suffered from poor potency and selectivity *in vitro*, leading to failure to further develop in drug discovery^{35–40}. Recently, we discovered a SIRT6 inhibitor, JYQ-42, that blocked the migration of BxPC-3 cells and the production of proinflammatory cytokines in a concentration-dependent manner⁴¹. However, the mediocre potency and limited drug-like properties prevented us from exploring the *in vivo* function of JYQ-42 at a safe dose. Therefore, potent and highly selective SIRT6 inhibitors are needed to explore the clinical applications of pharmacological SIRT6 inhibition in tumours such as pancreatic cancer.

Here, we developed a highly selective and potent inhibitor of SIRT6 by combining computational assistance and rational drug design. The allosteric binding site and the mechanism of allosteric inhibition were extensively elucidated by cocrystal complex structure and dynamic structural analyses. Importantly, we confirmed the antimetastatic function of such inhibitors in four pancreatic cancer cell lines and two mouse models of pancreatic cancer-induced liver metastasis. To our knowledge, this is the first study to reveal the *in vivo* pharmacological effects of SIRT6 inhibitors on pancreatic cancer metastasis, providing a valuable strategy to subsequently address the challenge of metastasis in pancreatic cancer.

2. Materials and methods

2.1. Protein expression and purification

The wild-type SIRT6 protein was constructed by direct insertion into the pET28a-His vector, and the point mutant protein was constructed using the Mut Express II Fast Mutagenesis Kit V2 (Vazyme), which were transformed into commercial receptive

Escherichia coli Rosetta (DE3) and cultured overnight on LB plates resistant to kanamycin. Single colonies were selected and cultured in 25 mL LB liquid medium with kanamycin resistance. After overnight culture, the cells were transferred to 1 L medium and cultured at 37 °C until the OD₆₀₀ value was about 0.8–1. After 0.5 mmol/L IPTG was added, the cells were induced at 16 °C for 16–18 h, collected by centrifugation at 4 °C, resuspended with lysis buffer (300 mmol/L NaCl; 5% glycerol; 1 mmol/L PMSF; 1× PBS; adjust the pH to 7.5), 1:1000 DTT and 1:100 Protease Inhibitor Cocktail in proportion. The WT or mutant SIRT6 protein was purified by Ni²⁺ column affinity chromatography and then centrifuged with SIRT6 assay buffer (50 mmol/L Tris-HCl; 137 mmol/L NaCl; 2.7 mmol/L KCl; 1 mmol/L MgCl₂, pH adjusted to 8.0) several times to replace the eluent to 1:1000.

2.2. FDL assays

The FDL assay was performed as described previously⁴². All compounds were dissolved with DMSO and diluted to the concentrations of 0.25, 1, 5, 20, 100, 100, 250, 500 μmol/L and 1 mmol/L. The 50 μL reaction system contained 5 μmol/L SIRT6, 2.5 mmol/L NAD⁺, 75 μmol/L RHKK-ac-AMC, 5 μL compounds/DMSO, and assay buffer. The reactions were conducted at 37 °C for 2.5 h, terminated with 40 mmol/L nicotinamide, and developed with 6 mg/mL trypsin for 30 min at 25 °C. The GraphPad Prism version 7.00 was used to fit the concentration-dependent curve and the IC₅₀ values were calculated from the dose–response equation. FDL assays for each compound were independently repeated at least three times.

2.3. HPLC assays

The HPLC assays of test compounds were performed as described previously⁴¹, with the concentration of protein and compound slightly adjusted. The 50 μL reaction mixture contained 20 μmol/L SIRT6 protein, 2.5 μmol/L NAD⁺, 5 μL DMSO or compound, and 75 μmol/L H3K9Ac peptide. The HPLC assays for each compound were independently repeated at least three times.

2.4. SPR assays

The SPR assays were performed on Biacore T200 instrument (GE Healthcare) as described previously with some changes⁴². Briefly, after immobilisation of His-SIRT6 on a CM5 sensor chip (GE) with an amine coupling kit (GE Healthcare), different concentrations of compound **11e** were infused into the flow system at 30 μL/min flow rate. Binding constants were analysed with the 1:1 Langmuir binding model in BIACORE T200 evaluation software v3.

2.5. Nucleosome assays

The nucleosome assays of test compounds were performed as described previously⁴¹ with some modifications. The reaction mixture of 40 μL included 4 μg mononucleosomes, 2 μg SIRT6, 2 mmol/L NAD⁺, and different concentrations of compounds or DMSO. After reaction at 37 °C for 30 min, the results were analysed by Western blot.

2.6. Selectivity assays

The selectivity assays of test compound on histone deacetylase enzymes (HDAC1–11, SIRT1–3) were performed by Eurofins

Cerep company (France) according to CEREP standard protocols. The enzymatic activity of SIRT6 was tested using the FDL assay described above.

2.7. Enzymatic kinetic assays

The enzymatic kinetic assays of the test compound were performed as described previously⁴¹ with some modifications. To determine the kinetics of peptide, 3.5 μmol/L SIRT6 was incubated with different concentrations (20–2500 μmol/L) of RHKK-Ac-AMC peptide in a 50 μL reaction mixture (2 mmol/L NAD⁺ and assay buffer) at 37 °C for 3 h (DMSO, 0.5 μmol/L compound), 5 h (1 μmol/L compound), or 7 h (2 μmol/L compound). For enzymatic kinetics of NAD⁺, 3.5 μmol/L SIRT6 was incubated with different concentrations (25–2000 μmol/L) of NAD⁺ in a 50 μL reaction mixture (640 μmol/L peptide and assay buffer) at 37 °C for 3 h (DMSO, 0.5 μmol/L compound), 5 h (1 μmol/L compound), or 7 h (2 μmol/L compound). The enzymatic kinetic assays for each compound were independently repeated at least three times.

2.8. Molecular dynamic (MD) simulations

Molecular simulations were performed based on our solved co-crystal structure of human SIRT6 with compound **11p** (PDB ID 8I2B), the position of substrate H3K9 myristoyl peptide was determined by our previous structure of SIRT6-substrate complex⁴² (PDB ID 5Y2F). To model the active reactant NAD⁺-bound SIRT6, the atomic coordinates of NAD⁺ were extracted from the co-crystal structure of SIRT1-NAD⁺ complex⁴³ (PDB ID 4I5I), and molecular docking was carried out using AutoDockFR–AutoDock⁴⁴ to position NAD⁺ into the active site of SIRT6. The structure of the Apo SIRT6 was obtained by manually deleting the compound **11p** coordinates from the complex crystal structure. The missing regions of the unsolved loop were reconstructed using MODELLER. The force field of acetyl-lysine residue and NAD⁺ were obtained from studies by Papamokos (<http://pc164.materials.uoi.gr/dpapeo/amberparams.php>) and AMBER parameter database (<http://amber.manchester.ac.uk/>), respectively. The zinc ion was managed using the cationic dummy atom (CADA)⁴⁵ approach proposed. The initial parameter files of conventional proteins and solvent molecules including ions were performed using ff14SB and tip3p force fields from Amber20 package^{46,47}. After semi-constrained (the proteins were position-constrained) and unconstrained energy minimization in turn, each system was heated to 300 K for 300 ps, then equilibrated at 300 K in a canonical ensemble for 1 ns. After all the preparations were completed, three independent rounds of 500 ns MD simulations were performed with random velocities for each system (for RMSD convergence, see Supporting Information Fig. S9). The dynamic network was built by NetworkView⁴⁸ plugin in VMD based on the correlation coefficient matrix. We used MMPBSA.py as implemented in the Amber20 package to calculate the Gibbs free energies of the binding process between SIRT6 and the acetylated peptide based on molecular mechanics Poisson-Boltzmann surface area.

2.9. Wound healing assays

Pancreatic cancer cells were seeded into each well of 6-well plates (2.5 × 10⁶) and incubated overnight. Cells were then cultured in a serum-free medium for 24 h. Wounds were made with RNase-free pipette tips (Axygen; AXY-T-300) and the cells were washed with

serum-free PBS. For BxPC-3 cells, PMA (30 ng/mL, final concentration) and a series of concentrations of **11e** were diluted in serum-free medium and added to wells. For other pancreatic cancer cells, a series of concentrations of **11e** were diluted in serum-free medium and added to wells. Photos were captured at indicated time point with a microscope (Leica, Wetzlar, Germany). The migration distances of cells were calculated by Image J and the relative migration rates were calculated as follows: (the distance of the wound at 0 – time point the distance of the wound at 24 h time point)/the distance of the wound at 0 time point⁴¹. ***P* < 0.01; ****P* < 0.001; *****P* < 0.0001, *t*-test (two-tailed and unpaired).

2.10. Transwell assays

The Transwell assay of pancreatic cancer cells was conducted using 24-well Transwell chambers which have upper and lower culture compartments (Costar, Cambridge, USA). The compartments were separated by polycarbonate membranes with 8 μm pores. For BxPC-3 cells, the bottom chamber was filled with medium containing 10% FBS, PMA (30 ng/mL, final concentration), and compound **11e** in different concentrations (0, 5, 10, 20 μmol/L). Cells in serum-free medium containing PMA (30 ng/mL, final concentration) and different concentrations of the compound **11e** (0, 5, 10, 20 μmol/L) were seeded at 6×10^4 in the top chamber and incubated in a humidified incubator containing 5% CO₂ at 37 °C. For other pancreatic cancer cells, the bottom chamber was filled with a medium containing 10% FBS and a series of concentrations of **11e**. Cells in serum-free medium containing different concentrations of the compound **11e** (0, 5, 10, 20 μmol/L) were seeded at 6×10^4 in the top chamber and incubated in a humidified incubator containing 5% CO₂ at 37 °C. The migrated cells in the underside of the membrane were stained with Trypan Blue solution. Images were captured by a microscope (Leica, Wetzlar, Germany).

2.11. Immunoblotting and antibodies

Pancreatic cancer cells were cultured with different concentrations of **11e** (0, 5, 10, 20 μmol/L) for 24 h. After treatment, total proteins were extracted by lysing cells with 1× SDS loading buffer. Protein samples were separated by 12% SDS-PAGE and transferred onto PVDF membranes. 5% nonfat milk in TBS-T was used for blocking. After blocking, membranes were incubated with primary antibody. 1% BSA in TBS-T was used to prepare primary and secondary antibodies. Protein bands were detected with G: BOX Chemi system (Syngene, Cambridge, UK).

The following antibodies were used: HRP-linked anti-rabbit IgG (Cell Signalling, 7074P2; 1:20,000); HRP-linked anti-mouse IgG (Cell Signalling, 7076P2; 1:20,000); SIRT6 (Cell Signalling, 12486; 1:2000); Histone H3 (Abcam, ab10799; 1:2000); Histone H3 (acetyl K9) (Abcam, ab32129; 1:1000); Histone H3 (acetyl K18) (Abcam, ab1191; 1:1000); Histone H3 (acetyl K56) (Active Motif, 39281; 1:1000); beta actin (Proteintech Group, HRP-60008; 1:5000).

2.12. Cell viability assays

Cells were seeded in 96-well plates at 8000 cells per well and incubated for 12 h. Then, compound **11e** in different concentrations (0.9375, 1.875, 3.75, 7.5, 15, 30, 60 μmol/L for HepG2 and SV-HUC-1; 100 μmol/L for other cells) were added to the

cultures. After 24 or 48 h, cell viability was measured by a Cell Counting Kit-8 (CCK-8) assay. Measurements were taken with a Synergy NEO microplate reader at 490 nm.

2.13. Tumour xenograft experiments

All animal experiments were performed following protocols approved by the Animal Ethics Committee of Shanghai Jiao Tong University. For the PANC-02 cell-driven xenograft tumour experiment, a total of 32 C57BL/6 mice were selected for the experiment and 8 mice from each group. For the L3.6pl cell-driven xenograft tumour experiment, a total of 12 BALB/c nude mice were selected for the experiment and 3 mice from each group. The mouse model of liver metastasis was established as described previously⁴⁹. After implantation of PANC-02 cells or L3.6pl cells (2×10^5 per mice) in the subcapsular region of the spleen of 4-week-old male C57BL/6 mice or BALB/c nude mice, followed by administered intraperitoneally 3, 10 and 30 mg/kg compound **11e** once daily for 28 days. The mice were sacrificed on Day 29 and the liver tissues were collected for subsequent pathological analysis.

2.14. PK study

The compound is prepared in 5% DMSO+10% Solutol+85% Saline to get the required solution for i.v., i.p., and *p.o.* administration in 12 male ICR mice of SPF. Each administration contains 3 treated mice and 1 control mouse. Before administration, the animals will be fasted overnight (10–16 h). Notably, food supply to the animals dosed orally will be resumed 4 h post-dose. At time points of 0.083, 0.25, 0.5, 1, 2, 4, 8 and 24 h after dosing for i.v. or 0.25, 0.5, 1, 2, 4, 6, 8 and 24 h after dosing for i.p. or 0.25, 0.5, 1, 2, 4, 6, 8 and 24 h after dosing for *p.o.*, the blood samples were collected from each animal *via* submandibular vein or other suitable vein, 0.03 mL/time point. The sample will be placed in tubes containing heparin sodium and stored on ice until centrifuged. The blood samples will be centrifuged at 6800×*g* for 6 min at 2–8 °C within 1 h after being collected and stored frozen at approximately –70 °C. The analytical results will be confirmed using quality control samples for intra-assay variation. The accuracy of >66.7% of the quality control samples should be between 80% and 120% of the known value(s). Standard set of parameters including Area Under the Curve (AUC_{0–t} and AUC_{0–∞}), elimination half-live (*t*_{1/2}), maximum plasma concentration (*C*_{max}), and time to reach maximum plasma concentration (*T*_{max}) will be calculated using noncompartmental analysis modules in FDA certified pharmacokinetic program Phoenix WinNonlin 7.0 (Pharsight, USA).

2.15. CYP inhibition assays

Pooled human liver microsomes (Cat. No. 452117) were purchased from BD Gentest. The liver microsomes were stored at –80 °C prior to use. DMSO and NADPH are purchased from Solarbio S&T Co., LTD. The incubation is carried out in 96 deep well plates. Dispense the following volumes into each well of the incubation plate: 169 μL of the master solution and 1 μL of the compound working solution or vehicle (acetonitrile). The incubation plate is placed into the water bath and pre-warmed at 37 °C for 5 min. Add 10 μL of substrate to the Incubation Plate, mix the incubation mixture on a whirly mixer for 15 s, and then add 20 μL of 10 mmol/L NADPH solution to start the reaction at the final

concentration of 1 mmol/L. After the addition of NADPH, the incubation plate is incubated at 37 °C. For CYP1A2, CYP2B6, CYP2C19, and CYP2D6 need to be incubated for 20 min, for CYP2C8, CYP2C9, and CYP3A4-M need to be incubated for 5 min, and for CYP2E1 need to be incubated for 10 min. Carry out the reaction in the 37 °C water bath for the appointed time. The assay is performed in duplicate. At the predetermined time points, quench the reaction by the addition of 300 μ L of quench solution (cold acetonitrile with 3% formic acid, 200 nmol/L alprazolam, 200 nmol/L labetalol, and 200 nmol/L tolbutamide) to each well. Centrifuge the plate at 3220 \times g for 40 min. Transfer 150 μ L of the supernatant to a new plate. The supernatant may be diluted with 150 μ L pure water. Mix well and analyse samples using UPLC–MS/MS.

2.16. Cell cycle assay

2×10^5 cells were placed in each well of the six-well plate and cultured overnight. After cell adhesion, compounds of different final concentrations (0, 5, 10, 20 μ mol/L) were added. After 24 h, the cells were digested, collected, and re-suspended with PBS. Cell Cycle Staining Kit (Multi Sciences) was used to detect cell cycle by flow cytometry (Beckman Coulter CytoFlex S).

2.17. Colony formation assay

The PANC-02 cells were seeded in 6-well plates at the density of 1000 cells per well. After 12 h, compound **11e** in different concentrations (0, 5, 10, 20 μ mol/L) were added for 10 days. Then the cell colonies were fixed with 4% paraformaldehyde for 20 min and then stained with crystal violet for 15 min. After washing three times with PBS, the number of colonies consisting of 50 or more cells was counted in each group.

2.18. Statistical analysis

GraphPad Prism software version 6.01 was performed for the statistical analyses. All data are presented as mean \pm standard deviation (SD) from at least three independent biological replicate experiments. Statistically significant differences between groups were defined (* $P < 0.05$; ** $P < 0.01$; *** $P < 0.001$; **** $P < 0.0001$).

3. Results

3.1. Structure-guide design of SIRT6 allosteric inhibitors

We used a combined computational and experimental approach to search for novel SIRT6 inhibitors. To increase the probability of identifying specific molecules, an allosteric pocket predicted by Allosite that is less conserved in the sirtuin family was chosen as the site for inhibitor screening^{42,50} (Fig. 1A). We then virtually docked more than 2,000,000 commercially available compounds into the allosteric site and purchased 20 compounds based on the top-ranked SIRT6–compound binding models to evaluate their inhibitory potency against SIRT6 deacetylation activity. Of these, compound **7** was identified as the hit, which had a half-maximal inhibitory concentration (IC₅₀) value of 76.42 ± 0.10 μ mol/L and a 54.9% inhibition ratio at 100 μ mol/L (Supporting Information Fig. S2A).

To further reveal the binding mode of compound **7**, we simulated the molecular conformation in the allosteric pocket (Fig. 1D). Phenyl ring A of compound **7** was inserted into the hydrophobic channel composed of Ile61, Phe64, Val70, Phe82, Phe86, and Val115 (Supporting Information Fig. S2B). The amino group failed to form hydrogen bonds with Pro62 or Asp116 due to lack of length. In addition, the nitro group is not surrounded by hydrogen bond donors that contribute to the affinity. In the solvent region, the group was shifted towards the gap composed of Trp71 and Met157 due to the flexibility of the middle linker. In a previous report, the amino acid residues at the bottom of the pocket were speculated to contribute to the affinity of general sirtuins, while the amino acid residues at the edge of the pocket may be related to the selectivity of sirtuin isomers⁵¹. Therefore, the structural optimization of phenyl ring A and phenyl ring B will be regarded as the main direction for subsequent modification to achieve potency and selectivity for SIRT6 (Fig. 1B and C).

First, we carried out a preliminary exploration of the structure–activity relationships (SARs) of the substituents on the phenyl ring A (Supporting Information Table S1). The monosubstituted derivatives **7a** and **7b** obtained by the removal of nitro or amino groups showed a marked decrease in inhibitory effect, while the lost potency was restored when an acetyl group was introduced over the amino group. Flipping the R₁ substituent of **7c** yielded the benzamide derivative **7d**, which exhibited moderate inhibitory activity against SIRT6 with an IC₅₀ value of 11.24 ± 1.85 μ mol/L.

Based on **7c**, we investigated the contribution of the R₂ substituent on phenyl ring B to SIRT6 inhibition. The replacement of hydrogen atoms by halogen atoms at the *ortho*-position (**8a–8c**) failed to improve the inhibitory potency, while the introduction of larger groups (**8d** and **8e**) resulted in a significant reduction in potency. At the *meta*-position, both electron-withdrawing groups (**8f** and **8j**) and hydrophobic groups (**8i** and **8j**) approximately doubled the inhibitory potency of the derivatives. Similarly, increasing the electron-withdrawing and hydrophobic ability of the *para*-substituents also improved the inhibition of the derivatives (**8p** and **8q**). Compared to the trifluoromethyl group (**8p**), the electron-donating ability of the methyl group (**8n**) and the hydrophilic ability of the cyanide group (**8q**) reduced the inhibitory potency of the derivatives by two- and threefold-fold, respectively. Based on the SARs of single substituents and the availability of synthetic materials, modifications with multiple substitutions in phenyl ring B were also attempted. Unfortunately, **8s** and **8t** showed little improvement in potency compared to the monosubstituted derivatives.

The amino acid residues that can form polar interactions, such as Ser56, Pro62, and Asn114, are mainly located at the bottom of the hydrophobic channel in the docking model; thus, we focused next on the modification of the amide group (Supporting Information Table S2). The replacement of amide groups with carboxylic acid (**7e**), methyl ester (**7f**), imidazole (**9c**), tetrazole (**9d**), or *N*-methylformamide (**9j**) led to a complete loss of inhibition, while groups where only the oxygen atom was replaced, such as thioamide (**9b**), methylamine (**9f**) and methylbenzylamine (**9g**), effectively maintained the inhibitory potency of the derivatives. Apparently, the nitrogen atom rather than the oxygen atom plays a major role in the formation of hydrogen bonds. In addition, the reduced potency caused by *meta*-methylamine (**9h**) or sulfonamide (**7g**) and the maintenance of potency caused by ethylamine (**9i**) suggest that the formation of hydrogen bonds requires a specific spatial conformation of the hydrogen bond

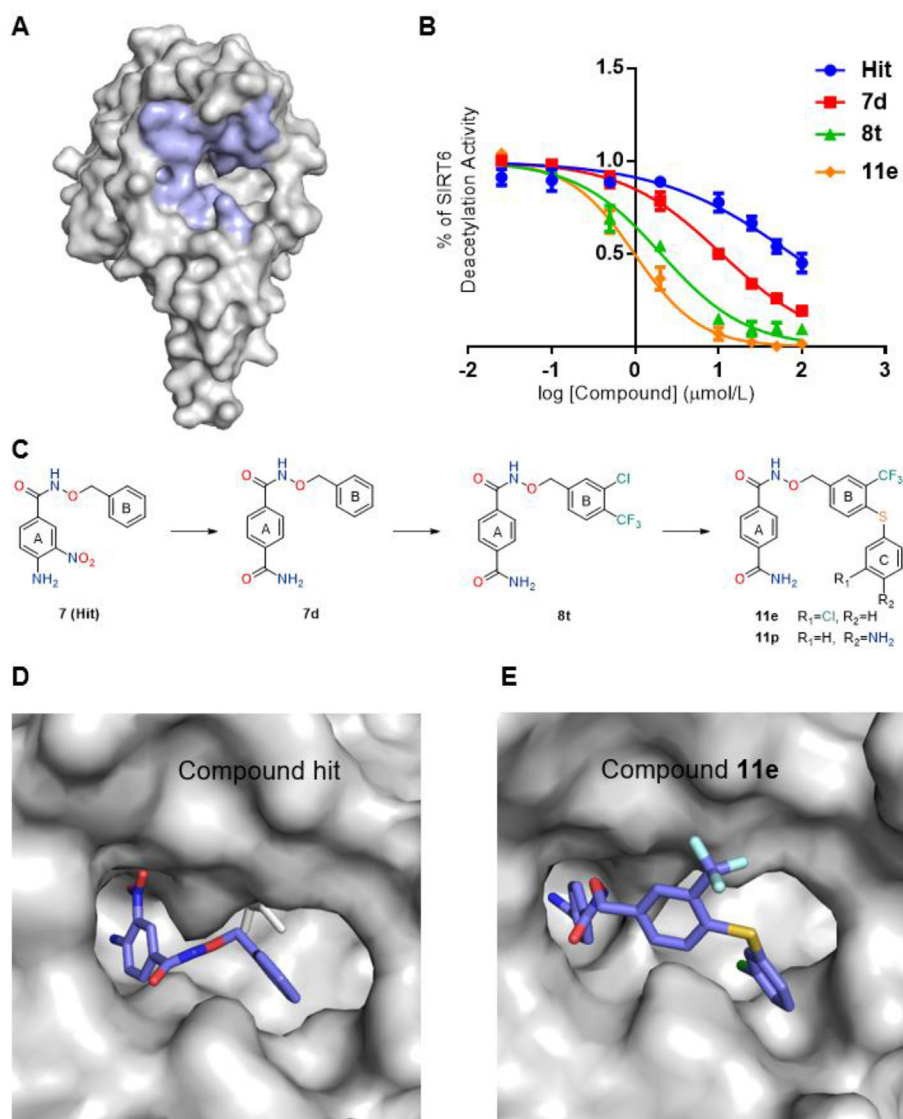


Figure 1 Discovery and optimization of novel inhibitors of SIRT6. (A) The allosteric site for virtual screening (PDB ID: 3PKI). (B) Dose–response curves of representative compounds in the optimization process. (C) Schematic overview of the optimization process. (D) Predicted binding mode of the hit compound with SIRT6. (E) Predicted binding mode of compound **11e** with SIRT6.

donor. This view was also supported by the decreased potency of **7e** and **9e**, which were generated by replacing the methyl group of **7d** with a carboxylic acid group and the amino group of **9f** with a hydroxyl group, respectively. Interestingly, a cyanide group (**9a**) and a hydroxamic acid group (**9k**) made the derivatives slightly less inhibitory, indicating the complexity of the allosteric effect at the bottom of the pocket. Taking into account both potency and druggability, we found no better substituent than the amide group.

In the SAR exploration of phenyl ring B, the replacement of the methyl group (**8n**) by a *tert*-butyl group (**8r**) caused a significant increase in the inhibitory potency of the derivatives, hinting at the possibility of a larger volume of *para*-substituents. Not entirely in line with our speculation, the addition of the aromatic ring (**10a–10j**) did not significantly improve the IC_{50} values of the derivatives, but the maximum inhibition rate increased from approximately 80% to almost 100% (Supporting Information Table S2). For the combination of potency, synthesis ability, and druggability, **10k** was used as the starting point for the next optimization. However, the substituents on the newly added

phenyl ring C exhibited a relatively small gap in potency, which is consistent with a previous report that the hydrophobic channel exit region might be associated with selectivity rather than affinity⁵¹ (Supporting Information Table S3). Remarkably, we found compound **11e** with an IC_{50} value of $0.98 \pm 0.13 \mu\text{mol/L}$, which is 78-fold more potent than the hit compound with an IC_{50} value of $76.42 \pm 0.10 \mu\text{mol/L}$ (Fig. 1B and E). To our knowledge, compound **11e** is the first inhibitor to exhibit sub-micromolar potency in enzymatic assays of SIRT6 *in vitro*.

3.2. Bioactivity verification and selectivity profiling of compound **11e**

To eliminate the risk of possible fluorescence interference in the FDL assay, high-performance liquid chromatography (HPLC) based on the H3K9Ac substrate peptide was used to further validate the authenticity of the inhibitory potency *in vitro* of compound **11e**. The results showed that the SIRT6 protein significantly removed acetyl groups from H3K9Ac, and this effect was

attenuated by compound **11e** in a dose-dependent manner (Fig. 2A). Given that SIRT6 exerts higher deacetylase activity *in vivo* than *in vitro* in a nucleosome-dependent manner⁵², we next examined whether the efficacy of the inhibitor was still applicable in nucleosomes. Consistent with the results of the assays on peptide substrates, compound **11e** effectively reversed the SIRT6-induced deacetylation of H3K9Ac and H3K18Ac (Fig. 2B). Moreover, surface plasmon resonance (SPR) suggested that compound **11e** exerts its inhibitory function by binding directly to SIRT6, with a K_d value of 9.46 $\mu\text{mol/L}$ (Fig. 2C and D). In addition to potency, precise selectivity is another major challenge in the development of sirtuin modulators⁵³. The inhibitory efficacy of compound **11e** against the other 14 members of HDACs was therefore assessed (Table 1). Encouragingly, compound **11e** did not affect the enzymatic activity of SIRT1, SIRT3, and HDAC1–11 at a concentration of 100 $\mu\text{mol/L}$. While compound **11e** inhibited SIRT2 with 21% potency at high concentrations, the weak effect failed to fit an IC_{50} curve. Overall, compound **11e** has a high selectivity for targeting SIRT6.

3.3. Binding mode of compound **11p**

We next attempted to explore the binding mode of these novel inhibitors through crystallography. Compound **11e** failed to form a complex with SIRT6 owing to its poor water solubility, but

the cocrystal complex structure of compound **11p** was solved at 2.20 Å resolution (Supporting information Table S4, PDB ID: 8I2B). Compound **11p**, an analogue of **11e**, showed slightly weaker inhibitory potency but superior water solubility (Supporting Information Table S3). Consistent with the docking model applied in the virtual screen, compound **11p** occupies the allosteric site located at the exit of the SIRT6 substrate acyl binding channel (Figs. 3A and 1D). The benzamide group inserted into a hydrophobic channel composed of Phe64, Phe82, Phe86, and Ile61 and might form π -stacking interactions of variable strength with the phenyl rings of peripheral phenylalanines. The crucial hydrogen bond formed between the nitrogen atom of the amide and the carboxyl group on the side chain of Asp116 deep in the channel (Fig. 3B). The thioether structure was oriented towards the solvent region, where phenyl ring B and the trifluoromethyl group interact with Val70, Trp71, and Met157. To validate the binding site of the complex, we individually mutated key residues in this pocket and performed FDL assays (Fig. 3C). In agreement with the structural analysis, the mutation of Asp116 eliminated the inhibitory potency. In addition, mutation of phenylalanine revealed that Phe86 rather than Phe64 or Phe82 provides the major π -stacking effect.

We then overlapped the cocrystal complex structure of compound **11p** with two other solved complexes to investigate the binding mechanism. The models showed that the amide group of

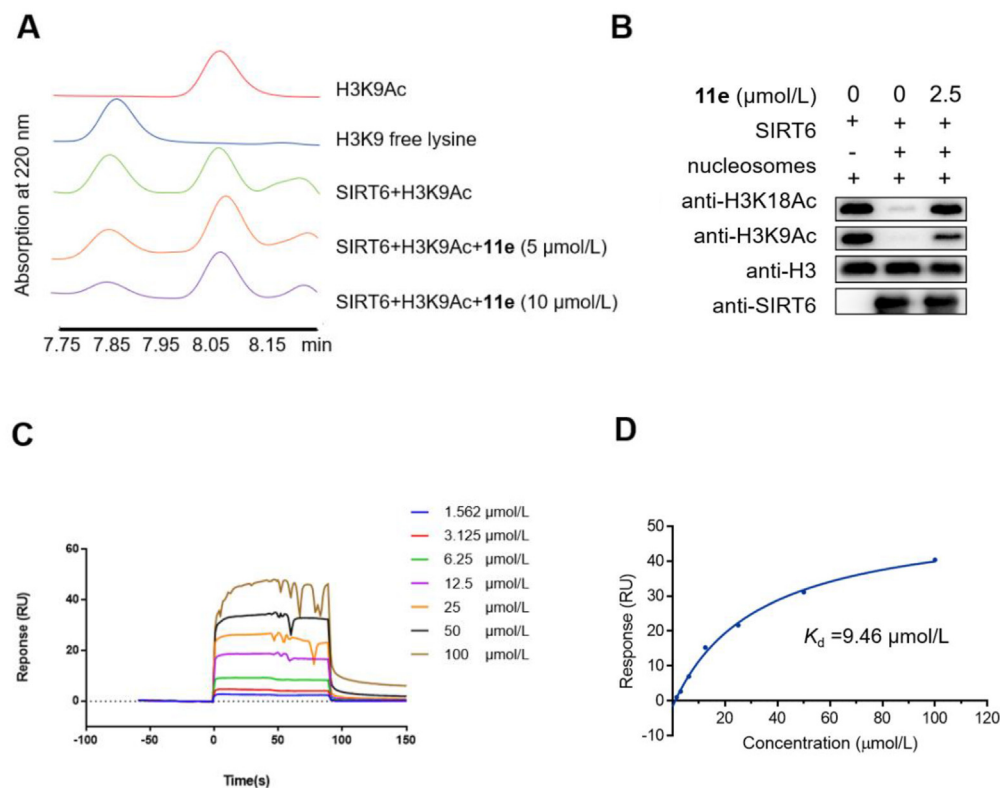


Figure 2 Biochemical characterization of compound **11e** as an inhibitor of SIRT6 deacetylation. (A) The effects of SIRT6 deacetylation on Ac-KQTARK-Ac-STGGWW-NH₂ in the absence or presence of 5 or 10 $\mu\text{mol/L}$ compound **11e**, as determined by HPLC. Data are representative of three independent experiments. (B) The effects of SIRT6 deacetylation on nucleosome substrates in the absence or presence of compound **11e**. Nucleosomes were extracted from HeLa cells, and the samples were analysed by Western blot analysis. Data are representative of three independent experiments. (C) The binding effect of compound **11e** on SIRT6 was measured by SPR. Three independent experiments were performed. (D) The steady-state affinity of binding compound **11e** to SIRT6. The K_d value of compound **11e** was 9.46 $\mu\text{mol/L}$, and three independent experiments were performed.

Table 1 Target selectivity of compound **11e** in the HDAC family.

| Enzyme | Inhibition rate (%) at 100 $\mu\text{mol/L}$ | Activity IC_{50} ($\mu\text{mol/L}$) ^a |
|--------|--|--|
| HDAC1 | 17.1 \pm 10.5 | NA |
| HDAC2 | 2.7 \pm 3.5 | NA |
| HDAC3 | 13.6 \pm 14.2 | NA |
| HDAC4 | 0.4 \pm 3.0 | NA |
| HDAC5 | 9.1 \pm 2.0 | NA |
| HDAC6 | 16.8 \pm 1.7 | NA |
| HDAC7 | 22.1 \pm 12.0 | NA |
| HDAC8 | 22.2 \pm 6.2 | NA |
| HDAC9 | -8.2 \pm 3.9 | NA |
| HDAC10 | 5.7 \pm 7.4 | NA |
| HDAC11 | -20.3 \pm 7.8 | NA |
| SIRT1 | -3.3 \pm 0.4 | NA |
| SIRT2 | 21.0 \pm 9.8 | NA |
| SIRT3 | 17.9 \pm 5.3 | NA |
| SIRT6 | 98.3 \pm 0.6 | 0.98 \pm 0.13 |

^aThe activity values are calculated based on IC_{50} for the inhibition effect. NA indicates inability to fit IC_{50} curves. Data are presented as the mean \pm SD from three independent experiments.

compound **11p** has an extremely similar conformation to the hydroxamate group of the inhibitor trichostatin A (Supporting Information Fig. S3A). Based on the hypothesis that the additional hydroxyl group of the hydroxamate might increase the affinity, we synthesized compound **9k** (Supporting Information

Table S2). Unfortunately, the inhibitory potency instead appeared to decrease, suggesting that the added interactions may be detrimental to the active conformation of the substrate site. Furthermore, the HDAC I/II members could be inhibited by trichostatin A but not compound **11e**, further supporting the strong correlation of the pocket edge with the selectivity of the sirtuin isoforms. Despite sharing the same binding site, the activator UBSC039 formed a critical hydrogen bond with amino acid Pro62 rather than Asp116 (Supporting Information Fig. S3B). The opposite effects triggered by Pro62 and Asp116 may help researchers to further understand the mechanism of remote allostery within this site.

3.4. Exploration of allosteric dynamic mechanisms

We next performed competition and enzyme kinetic experiments on the cofactor NAD^+ and the substrate peptide, confirming the above non-competitive binding mode revealed by crystallography from the perspective of enzyme function. In the catalytic reaction of SIRT6, the increased concentration of participants did not interfere with the inhibitory capacity of compound **11e**, indicating that this novel class of inhibitors is not in competition with cofactors or substrates (Fig. 4A–D). To uncover the allosteric mechanism of SIRT6 inhibition triggered by compound **11p**, we performed three independent rounds of 500 ns MD simulations of SIRT6- NAD^+ and the acetylated peptide substrate in the presence or absence of compound **11p**. We calculated the RMSD of the two most important domains as feature descriptors and generated the MD trajectories onto two-dimensional (2D) free energy

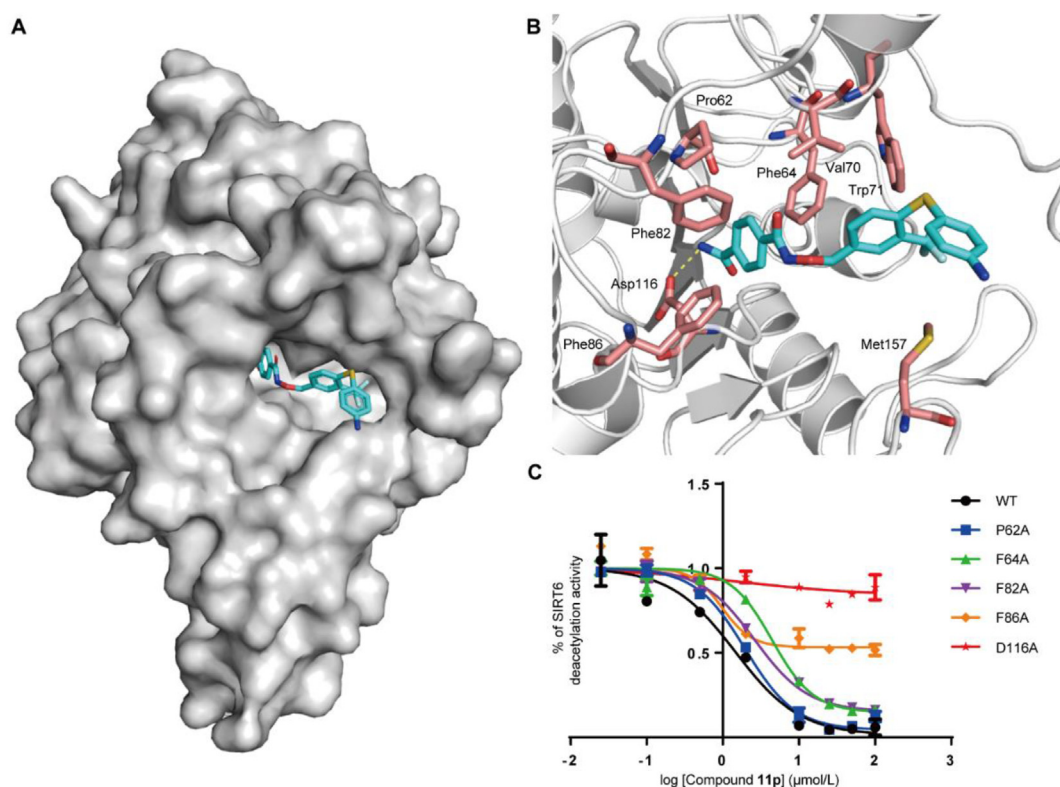


Figure 3 Crystal structure of compound **11p** in complex with SIRT6 (PDB ID: 8I2B). (A) Surface representation of compound **11p** bound to the allosteric site of SIRT6. SIRT6 is displayed as a grey surface, and compound **11p** is shown as cyan sticks. (B) Binding interactions between compound **11p** (carbon atoms: cyan) and SIRT6 (carbon atoms: salmon). The key residues are highlighted in stick representation. (C) Effects of site mutations located in the binding pocket on the inhibition of SIRT6 deacetylation, as determined by FDL assays.

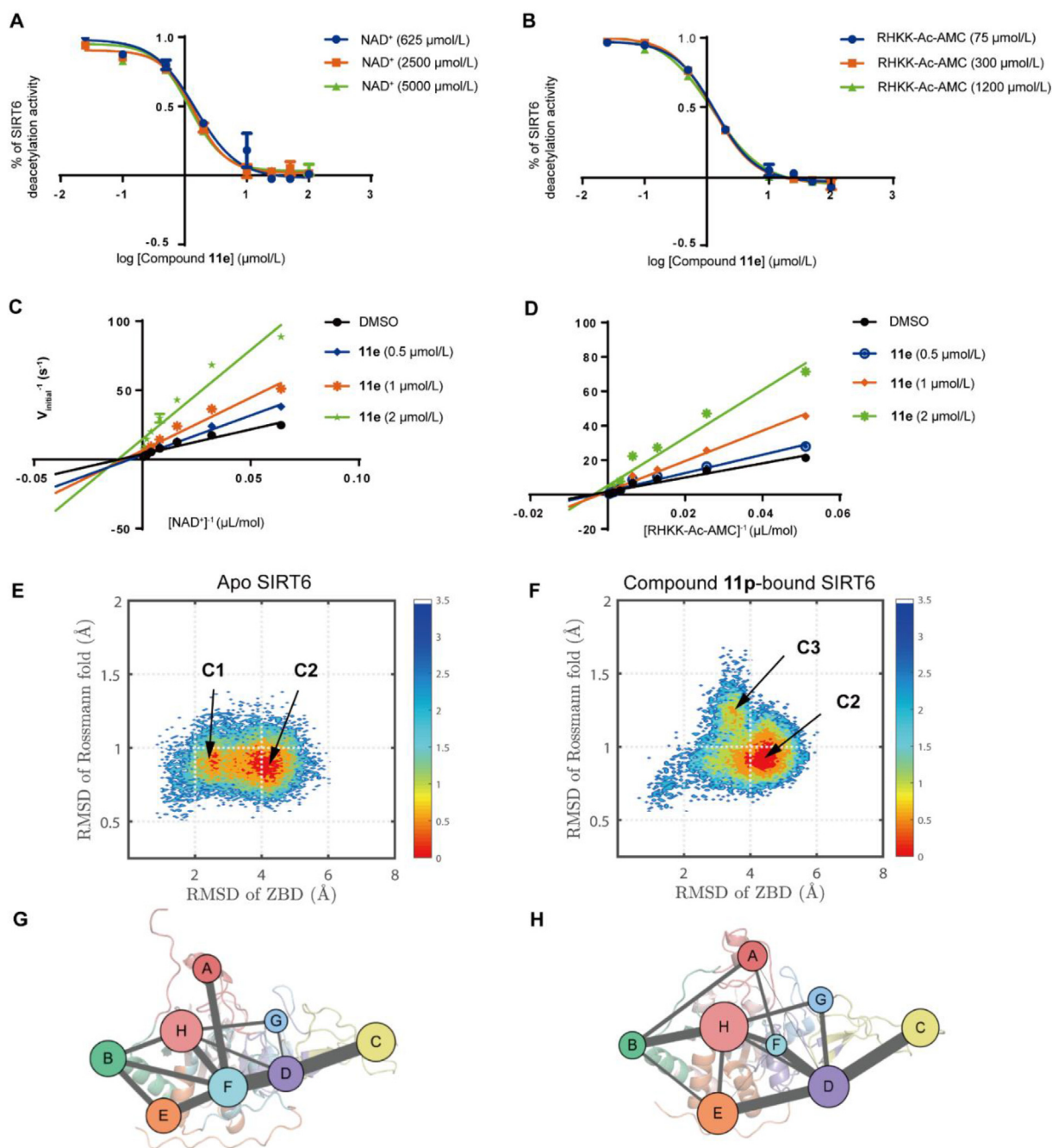


Figure 4 Mechanism of allosteric inhibition of SIRT6 by compound **11e** or **11p**. (A) Competitive relationship between compound **11e** and NAD^+ as determined by FDL assays. (B) Competitive relationship between compound **11e** and RHKK-Ac-AMC as determined by FDL assays. (C) Enzyme kinetics analysis of SIRT6 inhibition by compound **11e** with various concentrations of NAD^+ was conducted by HPLC. (D) Enzyme kinetics analysis of SIRT6 inhibition by compound **11e** with various concentrations of RHKK-Ac-AMC was conducted by HPLC. (E and F) Conformational landscapes of apo SIRT6 and compound **11p**-bound SIRT6 were generated using the RMSD of the Rossmann fold and zinc binding domain (ZBD) as the order parameters. The free energy values are reported in kcal/mol. (G and H) Map of the community network in compound **11p**-bound SIRT6. Areas of circles represent the numbers of residues in the corresponding communities, and the widths of sticks connecting communities represent the intercommunity connections.

landscapes (Fig. 4E and F). In the landscape, the conformations of the free energy basins were categorized as clusters C1–C3 according to their similar RMSD values. Both systems were mainly characterized by two conformations and shared a major free energy basin (C2). In addition, the binding of compound **11p** created

a novel free energy basin in C3 (Fig. 4F). The differential localization of C3 and the higher RMSD in the Rossmann fold suggested that compound **11p** caused a significant conformational change in SIRT6 and may mainly affect the stability of the NAD^+ and substrate binding sites.

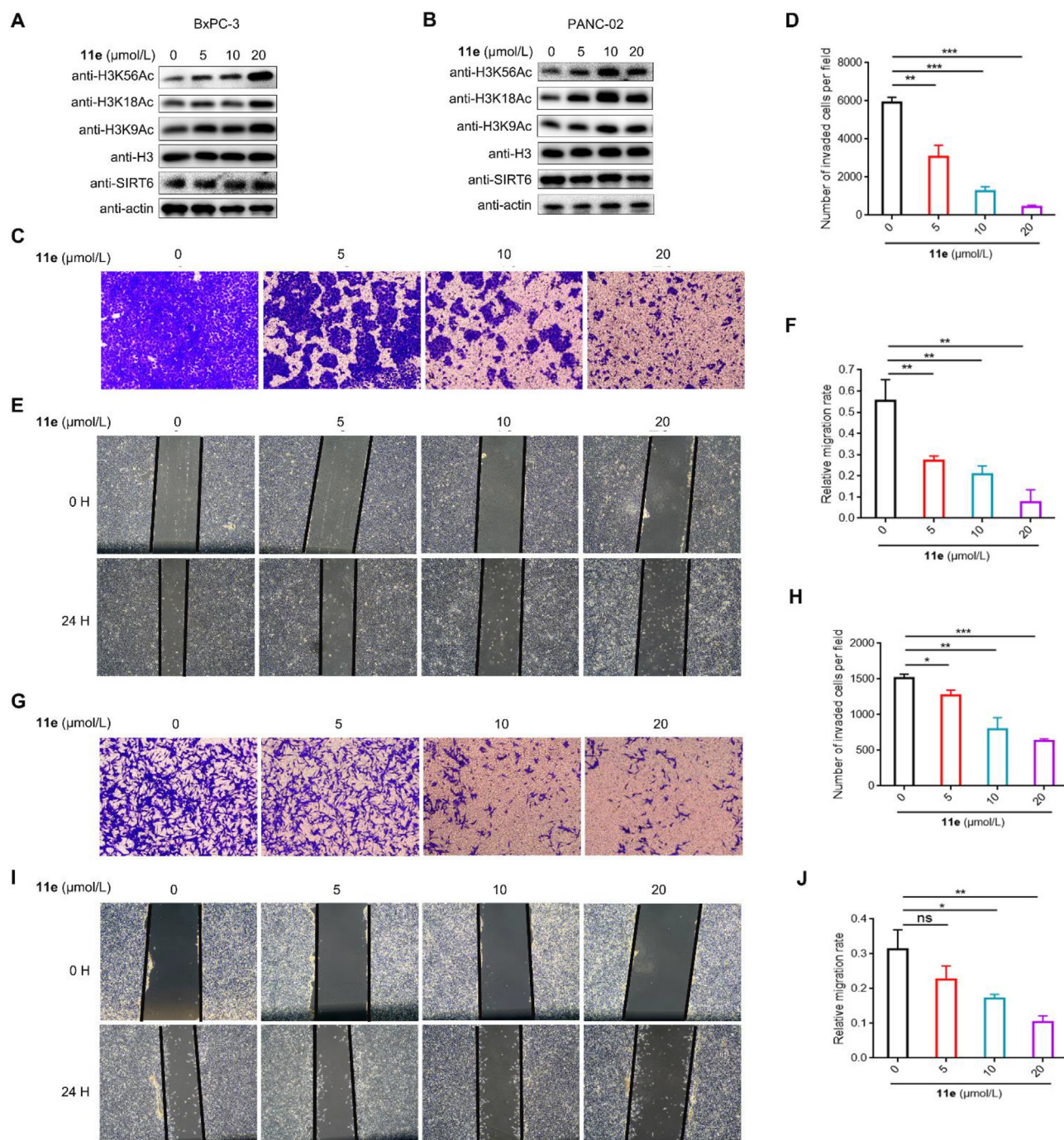


Figure 5 Compound **11e** inhibits the migration and SIRT6-mediated deacetylation of pancreatic cancer cells. (A) Western blot analysis of SIRT6 and its substrates H3K9Ac, H3K18Ac and H3K56Ac in BxPC-3 cells treated with the indicated compounds for 24 h. (B) Western blot analysis of SIRT6 and its substrates H3K9Ac, H3K18Ac and H3K56Ac in PANC-02 cells treated with the indicated compounds for 24 h. (C) Representative images of migrated BxPC-3 cells in the lower chambers following the Transwell assay. (D) Cell counting of migrated BxPC-3 cells in the lower chambers following Transwell assay. (E) Representative images of the wound healing assay of BxPC-3 cells treated with the indicated drugs at 0 and 24 h. (F) Relative migration rate in the wound healing assay of BxPC-3 cells treated with the indicated drugs at 0 and 24 h. (G) Representative images of migrated PANC-02 cells in the lower chambers following Transwell assay. (H) Cell counting of migrated PANC-02 cells in the lower chambers following Transwell assay. (I) Representative images of the wound healing assay of PANC-02 cells treated with the indicated drugs at 0 and 24 h. (J) Relative migration rate of wound healing assay of PANC-02 cells treated with the indicated drugs at 0 and 24 h. * $P < 0.05$, ** $P < 0.01$, *** $P < 0.001$, ns: no significance, t -test (two-tailed and unpaired).

Community network analysis was carried out to systematically investigate the communication between different regions across two systems to explore the propagation pathway of allosteric signals⁵⁴. There were eight communities in both the apo and compound **11p**-bound systems (Fig. 4G and H). The overall components of residues in the compound **11p**-bound system shifted from a relatively loose distribution to a concentration in three large groups (communities A, E and D) relative to the apo system, consistent with the system moving from a more flexible to a relatively stable state. Moreover, community F was no longer directly related to community B, and its association with other communities became weakened. Novel pathways were generated between communities A and B, communities A and D, communities D and E, and communities E and H (Fig. 4H). The above alteration of the community network suggests that compound **11p** could affect the activity of SIRT6 by weakening existing connections while generating new allosteric pathways. To further investigate allosteric communication from the compound **11p**-binding site to the substrate site, we calculated the Gibbs free energies of the binding process between SIRT6 and the acetylated peptide (Supporting Information Table S5). The analysis exhibited a free-energy decrease (~ 17 kcal/kmol) at the substrate site in response to compound **11p** binding, revealing the existence of allosteric coupling between the catalytic and compound **11p** sites. This result suggested that the binding of compound **11p** may reduce the stabilization of the activated conformation in the catalytic site, which is consistent with the experimentally observed reduction in SIRT6 deacetylation activity.

3.5. Bioactivities of compound **11e** in intact cells

After systematically exploring the *in vitro* pharmacological profiles, we then evaluated the inhibitory effect of compound **11e** on SIRT6 deacetylation in pancreatic cancer cells. In both the human-derived cell line BxPC-3 and the murine-derived cell line PANC-02, compound **11e** upregulated the acetylation levels of H3K9, H3K18, and H3K56 in a concentration-dependent manner (Fig. 5A and B). In addition, the abilities of both tumour cell lines to migrate were gradually decreased with increasing doses of compound **11e** (Fig. 5C–J). Notably, compound **11e** completely blocked the migration of BxPC-3 or PANC-02 cells at 20 $\mu\text{mol/L}$, while its inhibition of BxPC-3 migration at 10 $\mu\text{mol/L}$ reached that of JYQ-42 at 40 $\mu\text{mol/L}$ ⁴². In addition, we observed similar phenomena in two other human-derived pancreatic cancer cell lines, L3.6PL and SW1990, suggesting that compound **11e** indeed inhibits the migration of pancreatic cancer cells (Supporting Information Figs. S4 and S5). Considering that decreased cell viability also affects tumour cell migration, the survival rates of the above four cell lines cultured with high concentrations of compound **11e** were measured. Results showed that compound **11e** exhibited no cytotoxicity among the test cells at a concentration of 100 $\mu\text{mol/L}$ (Supporting Information Fig. S6). Moreover, the lack of cytotoxicity of the compound **11e** at a concentration of 60 $\mu\text{mol/L}$ to HepG2 cells and normal urothelial epithelial cell line SV-HUC-1 suggests a potential safety profile (Supporting Information Fig. S7). Interestingly, however, while compound **11e** did not affect the cell cycle of PANC-02 cells at 24 h, it produced a moderate reduction in colony formation in PANC-02 cells after 10 days of administration (Supporting Information Fig. S8). In summary, compound **11e** suppressed the migration of pancreatic cancer cells in a noncytotoxic manner at 24 h. Compared to JYQ-42, compound **11e** was a better probe

for the biological characterization and mechanistic investigation of SIRT6 inhibition at the cellular level.

3.6. Effect of SIRT6 inhibition in two mouse models of pancreatic cancer liver metastasis

Encouraged by the excellent *in vitro* efficacy, we attempted to evaluate the antitumour capacity of compound **11e** in the liver metastasis mouse model for pancreatic cancer. To determine the optimal route and dose of administration in animal assays, the pharmacokinetics of compound **11e** were studied in male ICR mice. Results showed that compound **11e** presented good absorption and rapid metabolism in three modes of administration, with intraperitoneal injection possessing the best half-life and moderate bioavailability (Table 2). Therefore, the intraperitoneal route of injection was used in the next animal experiments. We first evaluated the efficacy and safety of compound **11e** in a xenograft model constructed from mouse-derived pancreatic cancer cells PANC-02. After 28 days of administration, a reduction in liver metastatic nodules was observed compared with the control group in a concentration-dependent manner by treatment with compound **11e** (Fig. 6A and B). Promisingly, while the moderate dose of 10 mg/kg displayed marked inhibition of liver metastases, the high dose of 30 mg/kg showed no obvious weight loss or hepatotoxicity or renal toxicity (Fig. 6C–G). To further investigate the clinical potential of compound **11e**, we next repeated the above experiments in an animal model driven by the human-derived pancreatic cancer cell line L3.6pl. Consistent with the previous results, compound **11e** maintained an appreciable potency and safety profile (Fig. 7A–G). In particular, WB experiments showed that the levels of SIRT6 substrates H3K56Ac, H3K18Ac, and H3K56Ac increased *in vivo* with the concentration of compound **11e**, which are consistent with the results of the cellular experiments (Figs. 5A–B and 7H). This indicates that the suppression of pancreatic cancer metastasis *in vivo* by compound **11e** is also mediated through the inhibition of SIRT6. In conclusion, compound **11e** holds promise in the prevention of pancreatic cancer metastasis due to its combination of efficacy and safety.

4. Discussion

As one of the most aggressive malignancies, pancreatic cancer presents two major challenges: high metastasis and chemotherapy

Table 2 Pharmacokinetic parameters of compound **11e** in ICR mice ($n = 3$).

| PK parameter | i.v. (10 mg/kg) | i.p. (30 mg/kg) | <i>p.o.</i> (60 mg/kg) |
|-------------------------------|--------------------|--------------------|---------------------------|
| CL (mg/h/kg) | 684.42 | — | — |
| V_{ss} (mL/kg) | 92.94 | — | — |
| V_z (mL/kg) | 275.84 | — | — |
| $t_{1/2}$ (h) | 0.28 | 0.61 | 0.58 |
| T_{max} (h) | 0.08 | 0.42 | 0.25 |
| C_{max} (ng/mL) | 51,264.87 | 14,267.10 | 10,982.79 |
| AUC_{0-t} (h·ng/mL) | 14,631.11 | 24,489.55 | 8131.85 |
| $AUC_{0-\infty}$ (h·ng/mL) | 14,654.69 | 24,499.22 | 8169.86 |
| F (%) | — | 55.79 | 10.60 |

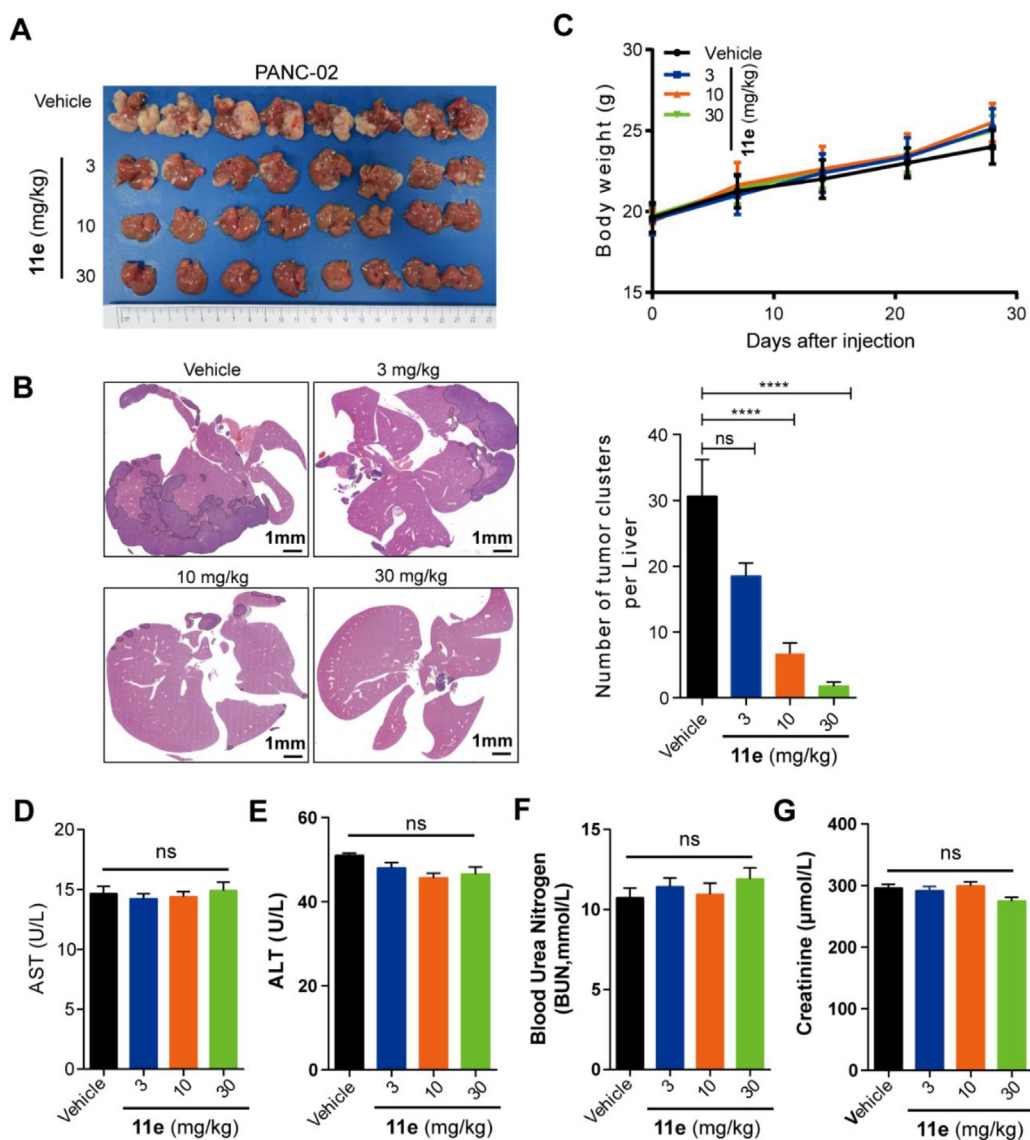


Figure 6 Compound **11e** inhibits the metastasis of mouse-derived pancreatic cancer cells in a dose-dependent manner *in vivo*. (A) Representative images of macroscopic metastatic lesions on the liver surface; white tissue indicates metastatic lesions. (B) Representative H&E staining and corresponding analysis of metastatic lesions. (C) Body weight change curves of the mice after different treatments. (D–G) The effect of compound **11e** on liver and kidney function in the liver metastasis model. AST, aspartate aminotransferase. ALT, alanine transaminase, $n = 8$ per group. **** $P < 0.0001$, ns: no significance, t -test (two-tailed and unpaired).

resistance^{24,55}. Compound **11e** has shown promising application in the treatment of metastatic pancreatic cancer *in vitro* and *in vivo*. Given that the SIRT6 inhibitors also exhibited the chemosensitizing effect in previous reports^{38,39}, the combination of compound **11e** with chemotherapeutic agents may have the potential to address both challenges. The excellent properties of compound **11e** in the CYP inhibition assays provided the basis for further drug combinations (Supporting Information Table S6). In particular, SIRT6 is also upregulated in other solid tumours, such as prostate, breast, and skin cancers. Compound **11e**, as the first SIRT6 inhibitor combining selectivity and antitumour function *in vivo*, holds promise for use in therapeutic strategies for a wider range of tumour indications. In addition, we obtained the first cocrystal complex structure of a synthetic SIRT6 inhibitor. The previously available complexes of only natural products with

SIRT6 could not effectively guide the development of novel inhibitors due to the synthetic difficulty of derivatives. With a relatively accessible synthetic route and large scope for modification, the optimization of compound **11e** is highly scalable.

Despite these advances, several challenges remain to be addressed. The first is that compound **11e** is currently metabolized too rapidly. We speculated that the middle linker between phenyl rings A and B is easily broken. A promising strategy for the next step of optimization is to improve the stability of the middle linker while maintaining the binding pose, thus increasing the half-life of the molecule. Moreover, a moderate reduction in colony formation of PANC-02 was observed after 10 days of prolonged administration of compound **11e**. We hypothesised that if PANC-02 cells were treated with **11e** for a long time (like 10 days for colony formation assay), **11e** could inhibit the proliferation of cancer

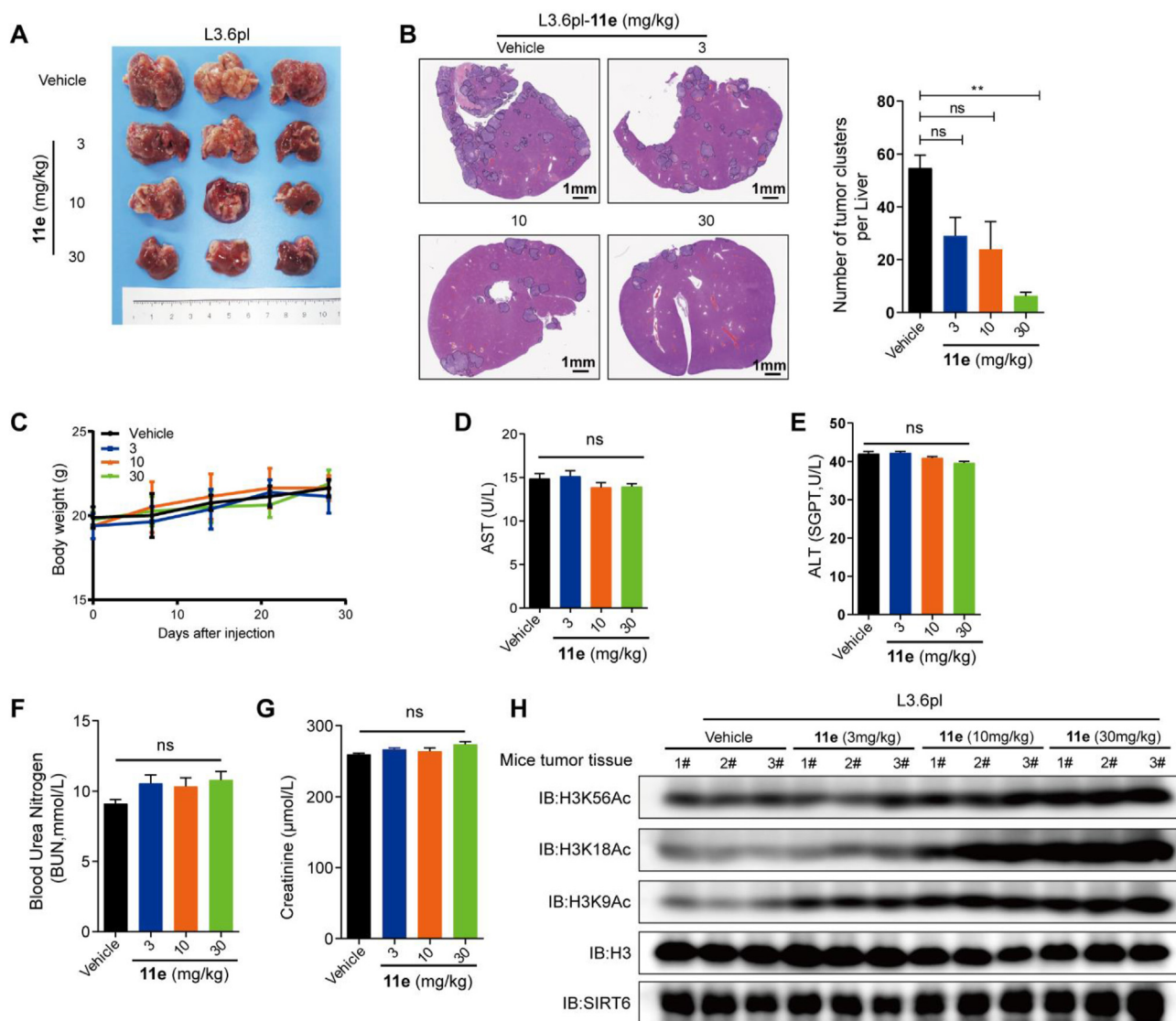


Figure 7 Compound **11e** inhibits the metastasis of human-derived pancreatic cancer cells in a dose-dependent manner *in vivo*. (A) Representative images of macroscopic metastatic lesions on the liver surface; white tissue indicates metastatic lesions. (B) Representative H&E staining and corresponding analysis of metastatic lesions. (C) Body weight change curves of the mice after different treatments. (D–G) The effect of compound **11e** on liver and kidney function in the liver metastasis model. AST, aspartate aminotransferase. ALT, alanine transaminase, $n = 8$ per group. $**P < 0.01$, ns: no significance, t -test (two-tailed and unpaired). (H) Western blot analysis of SIRT6 and its substrates H3K56Ac, H3K18Ac and H3K9Ac in three representative xenograft tumours from each group.

cells. The deeper mechanism requires further subsequent exploration. Finally, the cocrystal complex structure cannot fully reflect the SAR of the substituents on phenyl ring C. Due to the flexibility of the middle linker and thioether bond, the structure obtained by X-ray crystallography may not represent the conformation with the highest potency. Future inhibitor development could attempt to balance the rigidity and water solubility of the molecules to obtain more accurate complex structures.

5. Conclusions

In summary, we characterized the antimetastatic efficacy of the pharmacological inhibition of SIRT6 *in vivo* for the first time in the context of pancreatic cancer through the development of a potent and highly selective inhibitor of SIRT6. This inhibitor not

only offers a new therapeutic strategy to overcome metastasis in pancreatic cancer but also provides a promising chemical probe to explore the clinical applications of SIRT6 in other highly expressed cancers. The first cocrystal complex structure of a synthetic inhibitor of SIRT6 and the simplicity of synthesis also laid the foundation for further drug development.

Acknowledgments

This work was supported by the National Key R&D Program of China (grant no. 2022YFF1203005) the National Natural Science Foundation of China (22237005, 81903458, 82273425), Innovative research team of high-level local universities in Shanghai (SHSMU-ZDCX20212700, China), China Postdoctoral Science Foundation (2019M660090).

Author contributions

Jian Zhang, Qiufen Zhang, and Xuefeng Lu conceived and directed the project. Xinyuan Xu and Mingzhu Zhao contributed to the design and chemical synthesis of compounds. Xinyuan Xu, Qian Zhang, and Qiufen Zhang contributed to the *in vitro* biology experiments and data analysis. Yan Zheng and Xufeng Wang contributed to the *in vivo* biology experiments and data analysis. Yi Wang and Jing Jin contributed to the cocrystal. Chengwei Wu contributed to the dynamics simulation. Xinyuan Xu, Li Feng, and Jian Zhang wrote the manuscript. Xiuyan Yang, Yingyi Chen, Shaoyong Lu, Zhen Zheng, and Xiaobing Lan reviewed and edited the paper. All authors read and approved the final manuscript.

Conflicts of interest

There are no conflicts to declare.

Appendix A. Supporting information

Supporting data to this article can be found online at <https://doi.org/10.1016/j.apsb.2023.11.014>.

References

- Haberland M, Montgomery RL, Olson EN. The many roles of histone deacetylases in development and physiology: implications for disease and therapy. *Nat Rev Genet* 2009;**10**:32–42.
- Wu QJ, Zhang TN, Chen HH, Yu XF, Lv JL, Liu YY, et al. The sirtuin family in health and disease. *Signal Transduct Target Ther* 2022;**7**:402.
- Michishita E, McCord RA, Berber E, Kioi M, Padilla-Nash H, Damian M, et al. SIRT6 is a histone H3 lysine 9 deacetylase that modulates telomeric chromatin. *Nature* 2008;**452**:492–6.
- Michishita E, McCord RA, Boxer LD, Barber MF, Hong T, Gozani O, et al. Cell cycle-dependent deacetylation of telomeric histone H3 lysine K56 by human SIRT6. *Cell Cycle* 2009;**8**:2664–6.
- Tasselli L, Xi Y, Zheng W, Tennen RI, Odrowaz Z, Simeoni F, et al. SIRT6 deacetylates H3K18ac at pericentric chromatin to prevent mitotic errors and cellular senescence. *Nat Struct Mol Biol* 2016;**23**:434–40.
- Kawahara TLA, Michishita E, Adler AS, Damian M, Berber E, Lin M, et al. SIRT6 links histone H3 lysine 9 deacetylation to NF- κ B-dependent gene expression and organismal life span. *Cell* 2009;**136**:62–74.
- Sebastián C, Zwaans BMM, Silberman DM, Gymrek M, Goren A, Zhong L, et al. The histone deacetylase SIRT6 is a tumor suppressor that controls cancer metabolism. *Cell* 2012;**151**:1185–99.
- Fiorentino F, Carafa V, Favale G, Altucci L, Mai A, Rotili D. The two-faced role of sirt6 in cancer. *Cancers* 2021;**13**:1–26.
- Korotkov A, Seluanov A, Gorbunova V. Sirtuin 6: linking longevity with genome and epigenome stability. *Trends Cell Biol* 2021;**31**:994–1006.
- Kuang J, Chen L, Tang Q, Zhang J, Li Y, He J. The role of SIRT6 in obesity and diabetes. *Front Physiol* 2018;**9**:1–9.
- Guo Z, Li P, Ge J, Li H. SIRT6 in aging, metabolism, inflammation and cardiovascular diseases. *Aging Dis* 2022;**13**:1787–822.
- Liu G, Chen H, Liu H, Zhang W, Zhou J. Emerging roles of SIRT6 in human diseases and its modulators. *Med Res Rev* 2021;**41**:1089–137.
- Marquardt JU, Fischer K, Baus K, Kashyap A, Ma S, Krupp M, et al. Sirtuin-6-dependent genetic and epigenetic alterations are associated with poor clinical outcome in hepatocellular carcinoma patients. *Hepatology* 2013;**58**:1054–64.
- Feng J, Yan PF, Zhao HY, Zhang FC, Zhao WH, Feng M. SIRT6 suppresses glioma cell growth via induction of apoptosis, inhibition of oxidative stress and suppression of JAK2/STAT3 signaling pathway activation. *Oncol Rep* 2016;**35**:1395–402.
- Fukuda T, Wada-Hiraike O, Oda K, Tanikawa M, Makii C, Inaba K, et al. Putative tumor suppression function of SIRT6 in endometrial cancer. *FEBS Lett* 2015;**589**:2274–81.
- Cagnetta A, Soncini D, Orecchioni S, Talarico G, Minetto P, Guolo F, et al. Depletion of SIRT6 enzymatic activity increases acute myeloid leukemia cells' vulnerability to DNA-damaging agents. *Haematologica* 2018;**103**:80–90.
- Yang J, Li Y, Zhang Y, Fang X, Chen N, Zhou X, et al. SIRT6 promotes tumorigenesis and drug resistance of diffuse large B-cell lymphoma by mediating PI3K/Akt signaling. *J Exp Clin Cancer Res* 2020;**39**:1–16.
- Garcia-Peterson LM, Ndiaye MA, Singh CK, Chhabra G, Huang W, Ahmad N. SIRT6 histone deacetylase functions as a potential oncogene in human melanoma. *Genes Cancer* 2017;**8**:701–12.
- Khongkow M, Olmos Y, Gong C, Gomesl AR, Monteiro LJ, Yagüe E, et al. SIRT6 modulates paclitaxel and epirubicin resistance and survival in breast cancer. *Carcinogenesis* 2013;**34**:1476–86.
- Liu Y, Xie QR, Wang B, Shao J, Zhang T, Liu T, et al. Inhibition of SIRT6 in prostate cancer reduces cell viability and increases sensitivity to chemotherapeutics. *Protein Cell* 2013;**4**:702–10.
- Lu CT, Hsu CM, Lin PM, Lai CC, Lin HC, Yang CH, et al. The potential of SIRT6 and SIRT7 as circulating markers for head and neck squamous cell carcinoma. *Anticancer Res* 2014;**34**:7137–43.
- Bauer I, Grozio A, Lasiglie D, Basile G, Sturla L, Magnone M, et al. The NAD⁺-dependent histone deacetylase SIRT6 promotes cytokine production and migration in pancreatic cancer cells by regulating Ca²⁺ responses. *J Biol Chem* 2012;**287**:40924–37.
- Zhou P, Li B, Liu F, Zhang M, Wang Q, Liu Y, et al. The epithelial to mesenchymal transition (EMT) and cancer stem cells: implication for treatment resistance in pancreatic cancer. *Mol Cancer* 2017;**16**:52.
- Keleg S, Büchler P, Ludwig R, Büchler MW, Friess H. Invasion and metastasis in pancreatic cancer. *Mol Cancer* 2003;**2**:1–7.
- Bibok A, Kis B, Kim DW, Malafa M. Minimally invasive image-guided therapy of primary and metastatic pancreatic cancer. *World J Gastroenterol* 2021;**27**:4322–41.
- Tsilimigras DI, Brodt P, Clavien PA, Muschel RJ, D'Angelica MI, Endo I, et al. Liver metastases. *Nat Rev Dis Primers* 2021;**7**:28.
- Siegel RL, Miller KD, Fuchs HE, Jemal A. Cancer statistics, 2021. *CA Cancer J Clin* 2021;**71**:7–33.
- Manji GA, Olive KP, Saenger YM, Oberstein P. Current and emerging therapies in metastatic pancreatic cancer. *Clin Cancer Res* 2017;**23**:1670–8.
- Egberts JH, Cloosters V, Noack A, Schniewind B, Thon L, Klose S, et al. Anti-tumor necrosis factor therapy inhibits pancreatic tumor growth and metastasis. *Cancer Res* 2008;**68**:1443–50.
- Shi Q, Abbruzzese JL, Huang S, Fidler IJ, Xiong Q, Xie K. Constitutive and inducible interleukin 8 expression by hypoxia and acidosis renders human pancreatic cancer cells more tumorigenic and metastatic. *Clin Cancer Res* 1999;**5**:3711–21.
- Fernando RI, Castillo MD, Litzinger M, Hamilton DH, Palena C. IL-8 signaling plays a critical role in the epithelial-mesenchymal transition of human carcinoma cells. *Cancer Res* 2011;**71**:5296–306.
- Prevarskaya N, Skryma R, Shuba Y. Calcium in tumour metastasis: new roles for known actors. *Nat Rev Cancer* 2011;**11**:609–18.
- Bolívar BE, Welch JT. Studies of the binding of modest modulators of the human enzyme, sirtuin 6, by STD NMR. *ChemBioChem* 2017;**18**:931–40.
- Wood M, Rymarchyk S, Zheng S, Cen Y. Trichostatin A inhibits deacetylation of histone H3 and p53 by SIRT6. *Arch Biochem Biophys* 2018;**638**:8–17.
- Parenti MD, Grozio A, Bauer I, Galeno L, Damonte P, Millo E, et al. Discovery of novel and selective SIRT6 inhibitors. *J Med Chem* 2014;**57**:4796–804.

36. Sociali G, Magnone M, Ravera S, Damonte P, Vigliarolo T, von Holtey M, et al. Pharmacological SIRT6 inhibition improves glucose tolerance in a type 2 diabetes mouse model. *FASEB J* 2017;**31**:3138–49.
37. Liu J, Zheng W. Cyclic peptide-based potent human SIRT6 inhibitors. *Org Biomol Chem* 2016;**14**:5928–35.
38. Damonte P, Sociali G, Parenti MD, Soncini D, Bauer I, Boero S, et al. SIRT6 inhibitors with salicylate-like structure show immunosuppressive and chemosensitizing effects. *Bioorg Med Chem* 2017;**25**:5849–58.
39. Sociali G, Galeno L, Parenti MD, Grozio A, Bauer I, Passalacqua M, et al. Quinazolinone SIRT6 inhibitors sensitize cancer cells to chemotherapeutics. *Eur J Med Chem* 2015;**102**:530–9.
40. Sun W, Chen X, Huang S, Li W, Tian C, Yang S, et al. Discovery of 5-(4-methylpiperazin-1-yl)-2-nitroaniline derivatives as a new class of SIRT6 inhibitors. *Bioorg Med Chem Lett* 2020;**30**:127215.
41. Zhang Q, Chen Y, Ni D, Huang Z, Wei J, Feng L, et al. Targeting a cryptic allosteric site of SIRT6 with small-molecule inhibitors that inhibit the migration of pancreatic cancer cells. *Acta Pharm Sin B* 2022;**12**:876–89.
42. Huang Z, Zhao J, Deng W, Chen Y, Shang J, Song K, et al. Identification of a cellularly active SIRT6 allosteric activator. *Nat Chem Biol* 2018;**14**:1118–26.
43. Zhao X, Allison D, Condon B, Zhang F, Gheyi T, Zhang A, et al. The 2.5 Å crystal structure of the SIRT1 catalytic domain bound to nicotinamide adenine dinucleotide (NAD⁺) and an indole (EX527 analogue) reveals a novel mechanism of histone deacetylase inhibition. *J Med Chem* 2016;**59**:2267.
44. Ravindranath PA, Forli S, Goodsell DS, Olson AJ, Sanner MF. AutoDockFR: advances in protein-ligand docking with explicitly specified binding site flexibility. *PLoS Comput Biol* 2015;**11**:1–28.
45. Tang J, Park JG, Millard CB, Schmidt JJ, Pang YP. Computer-aided lead optimization: improved small-molecule inhibitor of the zinc endopeptidase of botulinum neurotoxin serotype A. *PLoS One* 2007;**2**.
46. Maier JA, Martinez C, Kasavajhala K, Wickstrom L, Hauser KE, Simmerling C. ff14SB: improving the accuracy of protein side chain and backbone parameters from ff99SB. *J Chem Theory Comput* 2015;**11**:3696–713.
47. Maier JA, Martinez C, Kasavajhala K, Wickstrom L, Hauser KE, Simmerling C, et al. Comparison of simple potential functions for simulating liquid water. *J Chem Theory Comput* 1983;**79**:926–35.
48. Eargle J, Luthey-Schulten Z. Network view: 3D display and analysis of protein-rNA interaction networks. *Bioinformatics* 2012;**28**:3000–1.
49. Zheng Y, Wu C, Yang J, Zhao Y, Jia H, Xue M, et al. Insulin-like growth factor 1-induced enolase 2 deacetylation by HDAC3 promotes metastasis of pancreatic cancer. *Signal Transduct Target Ther* 2020;**5**:1–14.
50. Huang W, Lu S, Huang Z, Liu X, Mou L, Luo Y, et al. Allosite: a method for predicting allosteric sites. *Bioinformatics* 2013;**29**:2357–9.
51. You W, Steegborn C. Structural basis of sirtuin 6 inhibition by the hydroxamate trichostatin A: implications for protein deacetylase drug development. *J Med Chem* 2018;**61**:10922–8.
52. Gil R, Barth S, Kanfi Y, Cohen HY. SIRT6 exhibits nucleosome-dependent deacetylase activity. *Nucleic Acids Res* 2013;**41**:8537–45.
53. Dai H, Sinclair DA, Ellis JL, Steegborn C. Sirtuin activators and inhibitors: promises, achievements, and challenges. *Pharmacol Ther* 2018;**188**:140–54.
54. Newman MEJ. Modularity and community structure in networks. *Proc Natl Acad Sci U S A* 2006;**103**:8577–82.
55. Yu S, Zhang C, Xie KP. Therapeutic resistance of pancreatic cancer: roadmap to its reversal. *Biochim Biophys Acta Rev Cancer* 2021;**1875**:188461.